Inorg. Chem. **2006**, *45*, 7197−7209

A Model Iridium Hydroformylation System with the Large Bite Angle Ligand Xantphos: Reactivity with Parahydrogen and Implications for Hydroformylation Catalysis

Daniel J. Fox,[†] Simon B. Duckett,[‡] Christine Flaschenriem,[†] William W. Brennessel,[†] Jacob Schneider,[†] Ahmet Gunay,[†] and Richard Eisenberg*[,†]

Department of Chemistry, University of Rochester, Rochester, New York 14627, and Department of Chemistry, University of York, York YO10 5DD, U.K.

Received April 28, 2006

Iridium complexes containing the large bite angle bisphosphine ligand xantphos have been synthesized and their reactivity studied. Several of these complexes are the first reported Ir(xantphos) systems to be characterized by X-ray diffraction. Variable-temperature NMR spectroscopic studies of $IrI(CO)_2$(xantphos) (**1-I**) and $Ir(COEt)(CO)_2$-(xantphos) (**8**) show two separate dynamic processes in which the phosphorus donors and the backbone methyl groups of the xantphos ligand are exchanged. The addition of parahydrogen (*p*-H_2) to **1-I** leads to the formation of two dihydride isomers including one in which both hydride ligands are trans to the phosphorus donors, suggestive of an Ir(I) xantphos intermediate with the ligand chelated in a trans-spanning fashion (**2b**). The bromide and chloride Ir(I) analogues (**1-Br** and **1-Cl**) also form this isomer upon reaction with parahydrogen, with **1-Cl** yielding *only* this dihydride species. The trihydride complex $IrH_3(CO)$(xantphos) (**7**) has been prepared, and its exchange with free hydrogen at elevated temperature is confirmed by reaction with *p*-H_2. The hydride complexes $IrH(CO)_2$(xantphos) (**6**) and $IrH_3(CO)$(xantphos) (**7**), as well as the propionyl complex **8**, are modest catalysts for the hydroformylation of 1-hexene and styrene under mild conditions. The addition of *p*-H_2 to **8** permits direct observation of the propionyl dihydride species $IrH_2(COEt)(CO)$(xantphos) (**9**) under both thermal and photolytic conditions, as well as unusual but weak polarization of the aldehydic proton of the propanal product that forms upon reductive elimination from **9**.

Introduction

Hydroformylation is one of the largest-scale homogeneous catalytic industrial processes involving dihydrogen as a reactant.[1−9] As proposed by Wilkinson and co-workers for $RhH(CO)(PPh_3)_3$ in the late 1960s, the accepted mechanism for hydroformylation using metal phosphine homogeneous catalysts involves an acyl dihydride species as the final intermediate before aldehyde formation.[10−12] While relatively few hydroformylation studies employ iridium complexes as active catalysts,[13−15] such systems can be of value as stable

* To whom correspondence should be addressed. E-mail: eisenberg@chem.rochester.edu.
[†] University of Rochester.
[‡] University of York.

(1) Parshall, G. W.; Ittel, S. D. *Homogeneous Catalysis. The Applications and Chemistry of Catalysis by Soluble Transition Metal Complexes*, 2nd ed.; John Wiley & Sons: New York, 1992.
(2) Pruett, R. L. *Adv. Organomet. Chem.: Catal. Org. Synth.* **1979**, *17*, 1.
(3) Buisman, G. J. H.; Kamer, P. C. J.; van Leeuwen, P. W. N. M. *Tetrahedron: Asymmetry* **1993**, *4*, 1625−1634.
(4) van Koten, G.; van Leeuwen, P. W. N. M. In *Catalysis: An Integrated Approach*; van Santen, R. A., van Leeuwen, P. W. N. M., Moulijn, J. A., Averill, B. A., Eds.; Elsevier: Amsterdam, 1999; Vol. 123, pp 289−342.
(5) Ungvary, F. *Coord. Chem. Rev.* **2002**, *228*, 61−82.
(6) Riley, D. P.; Tremont, S. J. In *Mechanisms of Inorganic and Organometallic Reactions*; Twigg, M. V., Ed.; Plenum Press: New York, 1988; Vol. 5, pp 335−374.
(7) Buisman, G. J. H.; Martin, M. E.; Vos, E. J.; Klootwijk, A.; Kamer, P. C. J.; van Leeuwen, P. W. N. M. *Tetrahedron: Asymmetry* **1995**, *6*, 719−738.
(8) van Leeuwen, P. W. N. M.; Roobeek, C. F. *J. Organomet. Chem.* **1983**, *258*, 343−350.
(9) Cotton, F. A.; Wilkinson, G. *Advanced Inorganic Chemistry*, 5th ed.; John Wiley & Sons: New York, 1988.
(10) Evans, D.; Osborn, J. A.; Wilkinson, G. *J. Chem. Soc. A* **1968**, 3133−3142.
(11) Yagupsky, G.; Brown, C. K.; Wilkinson, G. *J. Chem. Soc. A* **1970**, 1392−1401.
(12) Brown, C. K.; Wilkinson, G. *J. Chem. Soc. A* **1970**, 2753−2764.
(13) Mieczynska, E.; Trzeciak, A. M.; Ziolkowski, J. J.; Kownacki, I.; Marciniec, B. *J. Mol. Catal. A* **2005**, *237*, 246−253.
(14) Moreno, M. A.; Haukka, M.; Pakkanen, T. A. *J. Catal.* **2003**, *215*, 325−331.
(15) Crudden, C. M.; Alper, H. *J. Org. Chem.* **1994**, *59*, 3091−3097.

10.1021/ic060731l CCC: $33.50
Published on Web 08/03/2006

models for reaction intermediates, and one example has permitted characterization of the putative acyl dihydride species in the form of $IrH_2(COEt)(CO)(dppe)$ (dppe = 1,2-bis(diphenylphosphino)ethane).[16] One measure of success in hydroformylation catalysis is the ratio of linear-to-branched (l/b) aldehyde products, and both Casey and van Leeuwen have shown that the use of large natural bite angle bidentate ligands in the catalysts yield higher l/b product ratios,[17−21] as well as more active catalysts,[18,19,22] than those containing chelating ligands with smaller natural bite angles. Xantphos (9,9-dimethyl-4,6-bis(diphenylphosphino)xanthene; bite angle = 111.7°)[23] is one of those large natural bite angle ligands used in rhodium hydroformylation catalysts,[19−21,24−26] and it has been examined in platinum hydroformylation catalysts as well.[27,28]

In this report, the syntheses of a series of iridium xantphos complexes, including propionyl species that model hydroformylation intermediates, are presented, and some of them are shown to be catalytically active for hydroformylation under relatively mild conditions. The ability of the xantphos ligand to chelate in a trans fashion is highlighted by the addition of parahydrogen (p-H_2) to $IrX(CO)_2$(xantphos) (**1-X**; X = I, Cl, Br), in which an unusual hydrogen addition product with both hydride ligands trans to the phosphine donors is formed. The reaction of a propionyl complex with p-H_2 also makes the observation of an acyl-dihydride species through parahydrogen-induced polarization (PHIP) and the detection of an unusual but weak one-hydrogen polarization (oneH−PHIP) in the product aldehyde possible. PHIP has been employed by us and others as a useful mechanistic probe for solution-phase reactions involving molecular hydrogen[29−34] including hydroformylation.[35−37]

Results and Discussion

Synthesis and Characterization of New Iridium(xantphos) Complexes. The new Ir(xantphos) complexes are synthesized, in most cases, using the same general procedures as those employed for the preparation of analogous Ir(dppe) complexes.[16,38,39] As shown in eq 1, the addition of a solution of xantphos in THF to a solution of $[Bu_4N][IrI_2(CO)_2]$[38] results in the formation of $IrI(CO)_2$(xantphos) (**1-I**). The distorted trigonal bipyramidal geometry of **1-I** is unambiguously established by an X-ray diffraction study that shows a structure in which one phosphine donor is in an axial position trans to a carbonyl ligand and the other phosphine is in the equatorial plane with iodide and the second carbonyl (Figure 1). The bromide analogue of **1-I**, $IrBr(CO)_2$(xantphos) (**1-Br**), was synthesized in the same manner as **1-I** from $[Bu_4N][IrBr_2(CO)_2]$, while the chloride analogue, $IrCl(CO)_2$(xantphos) (**1-Cl**), was prepared from $[Ir(COD)Cl]_2$[40] via the addition of xantphos and CO. X-ray diffraction studies of **1-Br** and **1-Cl** confirm their trigonal bipyramidal geometries, but their structures differ significantly from that of **1-I**. In both **1-Br** and **1-Cl**, the halide and one carbonyl ligand are in axial positions, while the two phosphine donors and the second carbonyl are equatorial. Disorder exists between the axial carbonyl and halide ligands in the two structures. In **1-Br**, with an 84:16 disorder, the dominant form has the halide on the same side of the molecule as the xantphos backbone (Figure 2), while in **1-Cl**, with an 85:15 disorder, the dominant form has the axial carbonyl on the same side as the xantphos backbone (Figure 3). In the structure of **1-Cl**, two of the xantphos phenyl groups are perfectly stacked with a separation of 3.6 Å, suggestive of π-stacking stabilization in the solid state. To our knowledge, these complexes are the first examples of Ir(xantphos) complexes to be characterized by X-ray diffraction. See Tables 1−4 for the crystallographic details of the three structures. The IR spectra of complexes **1-X** show two CO stretches (**1-I** ν_{CO} = 2029, 1948 cm^{-1}; **1-Br** ν_{CO} = 2023, 1950 cm^{-1}; **1-Cl** ν_{CO} = 2017, 1944 cm^{-1}), consistent with the X-ray structures.

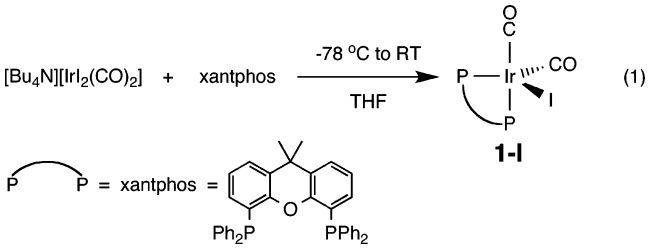

For complex **1-I**, the $^{31}P\{^1H\}$ and ^1H NMR spectra at −70 °C display, respectively, one sharp singlet at δ −13.5

(16) Deutsch, P. P.; Eisenberg, R. *Organometallics* **1990**, *9*, 709−718.
(17) Casey, C. P.; Whiteker, G. T.; Melville, M. G.; Petrovich, L. M.; Gavney, J. A.; Powell, D. R. *J. Am. Chem. Soc.* **1992**, *114*, 5535−5543.
(18) van der Veen, L. A.; Kamer, P. C. J.; van Leeuwen, P. W. N. M. *Organometallics* **1999**, *18*, 4765−4777.
(19) Freixa, Z.; van Leeuwen, P. W. N. M. *Dalton Trans.* **2003**, 1890−1901.
(20) Kamer, P. C. J.; van Leeuwen, P. W. N. M.; Reek, J. N. H. *Acc. Chem. Res.* **2001**, *34*, 895−904.
(21) van Leeuwen, P. W. N. M.; Kamer, P. C. J.; Reek, J. N. H.; Dierkes, P. *Chem. Rev.* **2000**, *100*, 2741−2769.
(22) Bronger, R. P. J.; Kamer, P. C. J.; van Leeuwen, P. W. N. M. *Organometallics* **2003**, *22*, 5358−5369.
(23) Kraneneburg, M.; van der Burgt, Y. E. M.; Kamer, P. C. J.; van Leeuwen, P. W. N. M.; Goubitz, K.; Fraanje, J. *Organometallics* **1995**, *14*, 3081−3089.
(24) Breit, B. *Acc. Chem. Res.* **2003**, *36*, 264−275.
(25) Trzeciak, A. M.; Ziolkowski, J. J. *Coord. Chem. Rev.* **1999**, *190−192*, 883−900.
(26) Landis, C. R.; Uddin, J. *J. Chem. Soc., Dalton Trans.* **2002**, 729−742.
(27) van der Veen, L. A.; Keeven, P. K.; Kamer, P. C. J.; van Leeuwen, P. W. N. M. *J. Chem. Soc., Dalton Trans.* **2000**, 2105−2112.
(28) Petocz, G.; Berente, Z.; Kegl, T.; Kollar, L. *J. Organomet. Chem.* **2004**, *689*, 1188−1193.
(29) Duckett, S. B.; Sleigh, C. J. *Prog. Nucl. Magn. Reson. Spectrosc.* **1999**, *23*, 71−92.
(30) Eisenberg, R. *Acc. Chem. Res.* **1991**, *24*, 110−116.
(31) Eisenberg, R.; Eisenschmid, T. C.; Chinn, M. S.; Kirss, R. U. *Adv. Chem. Ser.* **1992**, *230*, 47−74.
(32) Natterer, J.; Bargon, J. *Prog. Nucl. Magn. Reson. Spectrosc.* **1997**, *31*, 293−315.
(33) Bowers, C. R. In *Encyclopedia of Nuclear Magnetic Resonance*; Grant, D. M., Harris, R. K., Eds.; John Wiley & Sons: Chichester, U.K., 2002; Vol. 9 (Advances in NMR), pp 750−770.
(34) Duckett, S. B.; Blazina, D. *Eur. J. Inorg. Chem.* **2003**, 2901−2912.
(35) Permin, A. B.; Eisenberg, R. *J. Am. Chem. Soc.* **2002**, *124*, 12406−12407.
(36) Godard, C.; Duckett, S. B.; Henry, C.; Polas, S.; Toose, R.; Whitwood, A. C. *Chem. Commun.* **2004**, 1826−1827.
(37) Godard, C.; Duckett, S. B.; Polas, S.; Tooze, R.; Whitwood, A. C. *J. Am. Chem. Soc.* **2005**, *127*, 4994−4995.
(38) Albietz, P. J. PhD Thesis, University of Rochester, Rochester, NY, 2001.
(39) Fisher, B. J.; Eisenberg, R. *Organometallics* **1983**, *2*, 764−767.
(40) Herde, J. L.; Lambert, J. C.; Senoff, C. V. *Inorg. Synth.* **1974**, *15*, 18−20.

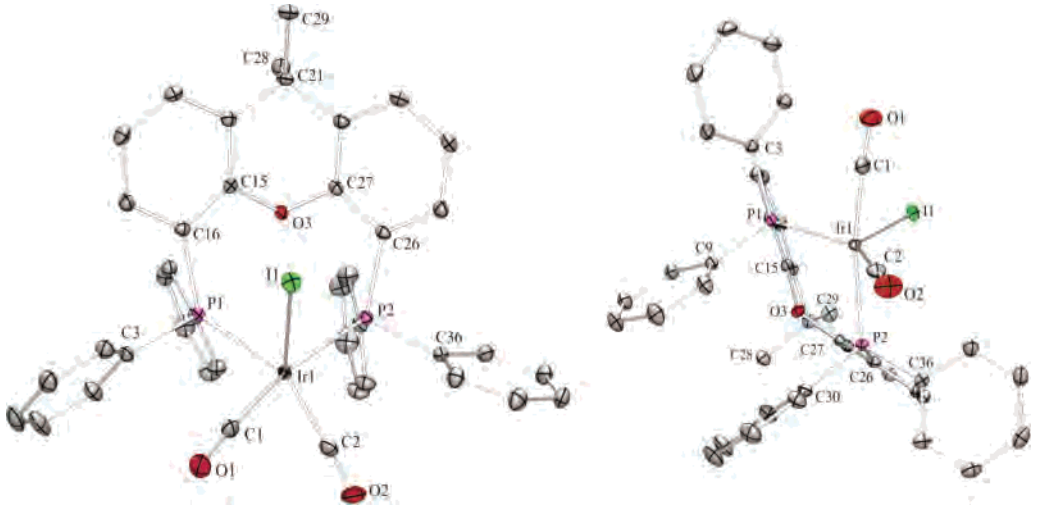

Figure 1. Two ORTEP views of **1-I** showing a partial labeling scheme; ellipsoids are at the 50% probability level. Hydrogen atoms have been removed for clarity.

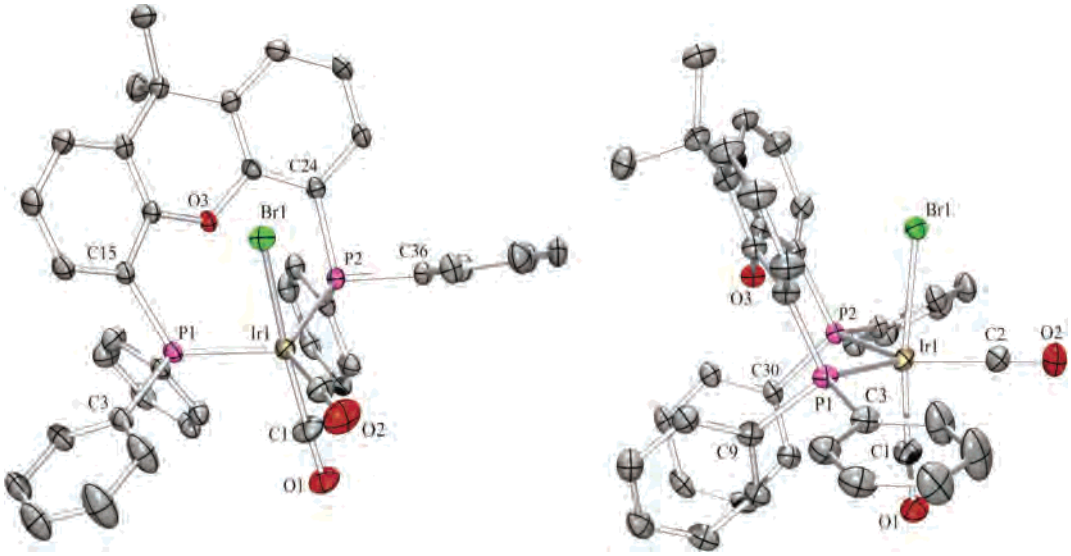

Figure 2. Two ORTEP views of **1-Br** showing a partial labeling scheme; ellipsoids are at the 50% probability level. Hydrogen atoms have been removed for clarity.

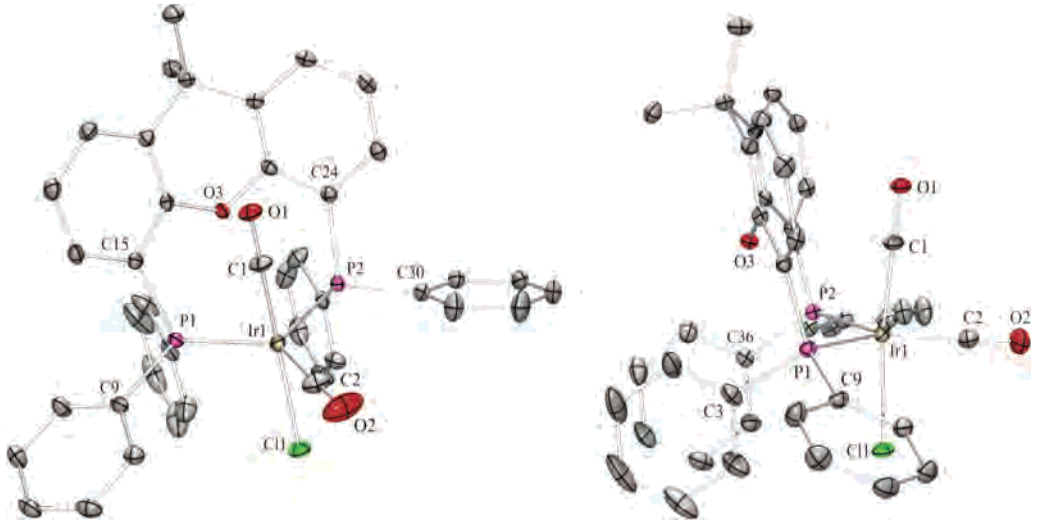

Figure 3. Two ORTEP views of **1-Cl** showing a partial labeling scheme; ellipsoids are at the 50% probability level. Hydrogen atoms have been removed for clarity.

Table 1. Crystallographic Data for $IrI(CO)_2$(xantphos) (**1-I**), $IrBr(CO)_2$(xantphos) (**1-Br**), $IrCl(CO)_2$(xantphos) (**1-Cl**), $IrH_2Cl(CO)$(xantphos) (**4-Cl**), and $Ir(COEt)(CO)_2$(xantphos) (**8**)

	1-I	1-Br	1-Cl	4-Cl	8
empirical formula	$C_{41}H_{32}IIrO_3P_2$	$C_{41}H_{32}BrIrO_3P_2$	$C_{41}H_{32}ClIrO_3P_2$	$C_{40}H_{34}ClIrO_2P_2$	$C_{54.5}H_{48}IrO_4P_2$
fw	953.71	906.72	862.26	836.26	1021.07
T (K)	100.0(1)	100.0(1)	100.0(1)	100.0(1)	100(2)
λ (Å)	0.71073	0.71073	0.71073	0.71073	0.71073
cryst syst	monoclinic	monoclinic	monoclinic	triclinic	triclinic
space group	$P2_1/c$	$P2_1/c$	$P2_1/c$	$P\bar{1}$	$P\bar{1}$
Z	4	4	4	2	2
a (Å)	17.5313(8)	17.034(2)	17.058(2)	9.8245(10)	10.207(2)
b (Å)	10.9903(5)	11.2558(13)	9.8230(12)	10.9194(11)	12.798(3)
c (Å)	18.3293(8)	20.251(2)	20.468(2)	17.7056(18)	18.194(4)
β (deg)	92.401(1)	90.457(2)	97.126(2)	75.507(1)	101.94(3)
V (Å^3)	3528.5(3)	3882.7(7)	3403.1(7)	1713.9(3)	2300.2(9)
ρ_{calcd} (Mg/m^3)	1.795	1.551	1.683	1.620	1.474
μ (mm^{-1})	4.788	4.585	4.136	4.101	3.018
abs correction	SADABS	SADABS	SADABS	SADABS	SADABS
transm range	0.1571−0.2674	0.4207−0.5261	0.3868−0.5652	0.3131−0.6189	0.3496−0.7893
F(000)	1848	1776	1704	828	1028
2θ range (deg)	2.16−30.03	2.01−32.58	2.01−30.51	2.00−30.51	1.15−29.57
limiting indices	$-24 \le h \le 24$ $-15 \le k \le 15$ $-25 \le l \le 25$	$-25 \le h \le 25$ $-16 \le k \le 17$ $-30 \le l \le 30$	$-24 \le h \le 24$ $-13 \le k \le 14$ $-28 \le l \le 29$	$-14 \le h \le 14$ $-15 \le k \le 15$ $-25 \le l \le 25$	$-24 \le h \le 24$ $-17 \le k \le 17$ $-24 \le l \le 25$
no. of reflns collected	52 260	68 408	52 021	28 003	34 426
no. of data/restraints/params	10 254/0/435	13 968/0/439	10 237/3/439	10 410/15/424	12 770/50/601
GOF	1.040	1.056	1.059	1.097	1.066
R1, wR2 ($I > 2\sigma$)	0.0148, 0.0351	0.0279, 0.0631	0.0188, 0.0444	0.0282, 0.0604	0.0365, 0.0995
R1, wR2 (all data)	0.0164, 0.0355	0.0374, 0.0653	0.0228, 0.0454	0.0301, 0.0611	0.0403, 0.0988

Table 2. Selected Bond Lengths (Å) and Angles (deg) for **1-I**

Ir(1)−C(2)	1.8611(17)	Ir(1)−I(1)	2.79885(16)
Ir(1)−C(1)	1.8942(17)	C(1)−O(1)	1.137(2)
Ir(1)−P(2)	2.3875(4)	C(2)−O(2)	1.154(2)
Ir(1)−P(1)	2.4221(4)		
C(2)−Ir(1)−C(1)	87.42(7)	C(2)−Ir(1)−I(1)	132.27(5)
C(2)−Ir(1)−P(2)	84.35(5)	C(1)−Ir(1)−I(1)	87.97(5)
C(1)−Ir(1)−P(2)	168.35(5)	P(2)−Ir(1)−I(1)	91.471(9)
C(2)−Ir(1)−P(1)	136.27(5)	P(1)−Ir(1)−I(1)	91.307(9)
C(1)−Ir(1)−P(1)	91.36(5)	O(1)−C(1)−Ir(1)	175.04(15)
P(2)−Ir(1)−P(1)	100.287(13)	O(2)−C(2)−Ir(1)	177.34(16)

Table 3. Selected Bond Lengths (Å) and Angles (deg) for the Major Form of **1-Br**

Ir(1)−C(1)	1.830(3)	Ir(1)−Br(1)	2.5253(4)
Ir(1)−C(2)	1.897(2)	C(1)−O(1)	1.163(4)
Ir(1)−P(2)	2.4063(6)	C(2)−O(2)	1.141(3)
Ir(1)−P(1)	2.4230(6)		
C(1)−Ir(1)−C(2)	88.42(14)	P(2)−Ir(1)−P(1)	103.03(2)
C(1)−Ir(1)−P(2)	93.21(11)	C(1)−Ir(1)−Br(1)	172.05(12)
C(2)−Ir(1)−P(2)	130.01(8)	C(2)−Ir(1)−Br(1)	83.84(7)
C(1)−Ir(1)−P(1)	94.43(12)	P(2)−Ir(1)−Br(1)	90.429(17)
C(2)−Ir(1)−P(1)	126.68(8)	P(1)−Ir(1)−Br(1)	91.631(16)

Table 4. Selected Bond Lengths (Å) and Angles (deg) for the Major Form of **1-Cl**

Ir(1)−C(1)	1.865(3)	Ir(1)−P(1)	2.4174(5)
Ir(1)−C(2)	1.881(2)	C(1)−O(1)	1.152(3)
Ir(1)−Cl(1)	2.3900(6)	C(2)−O(2)	1.145(2)
Ir(1)−P(2)	2.4131(5)		
C(1)−Ir(1)−C(2)	87.73(10)	Cl(1)−Ir(1)−P(2)	93.364(18)
C(1)−Ir(1)−Cl(1)	172.29(8)	C(1)−Ir(1)−P(1)	92.52(8)
C(2)−Ir(1)−Cl(1)	85.09(6)	C(2)−Ir(1)−P(1)	137.38(7)
C(1)−Ir(1)−P(2)	92.87(8)	Cl(1)−Ir(1)−P(1)	90.862(18)
C(2)−Ir(1)−P(2)	122.56(7)	P(2)−Ir(1)−P(1)	100.008(18)

(Figure 4) and a substantially broadened (or coalesced) xantphos methyl resonance, indicative of dynamic behavior of the complex. At ambient temperature, a single broad resonance is seen in the $^{31}P\{^1H\}$ NMR spectrum at δ −13.5.

Scheme 1

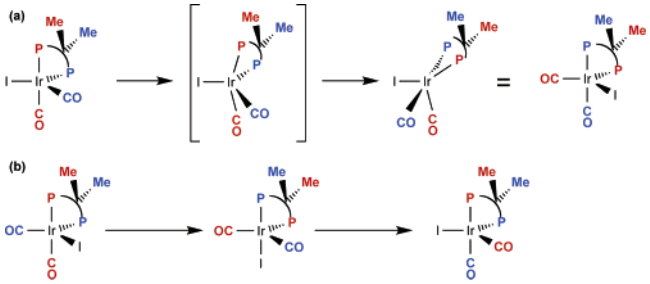

(a) One Berry pseudorotation using iodide as pivot to equilibrate the phosphine donors with intermediate shown. **(**b) Two Berry pseudorotations using the two CO ligands as consecutive pivots to equilibrate Me and Me.

In light of the structure determined for **1-I** by crystallography and the variable-temperature NMR experiments, the fluxional behavior of **1-I** can be explained by consideration of the two separable dynamic processes corresponding to Berry pseudorotation and intermolecular exchange. At low temperature, Berry pseudorotation using the Ir−I bond as the "pivot" exchanges the two phosphine donors (Scheme 1a), while successive pseudorotations using the two carbonyl ligands as "pivots" exchange the two inequivalent methyl groups on the xantphos backbone (Scheme 1b). A second, higher activation barrier process also takes place that involves the loss of CO followed by re-coordination of CO and accounts for the broad single ^{31}P resonance seen between 0 and 30 °C and its sharpening as the temperature is increased. The feasibility of CO loss and re-coordination is confirmed by exchange with ^{13}CO at ambient temperature: as shown in the inset of Figure 4, the ^{31}P resonance of **1** shows coupling to two ^{13}C nuclei at −50 °C. A similar combination of low-temperature pseudorotations and higher-temperature intermolecular exchange has been used to rationalize the dynamic behavior of the related 5-coordinate Ir(I) complex $Ir(CO)(\eta^2\text{-}C_2H_4)_2(dppe)^+$.[41] An alternative mechanism can also be

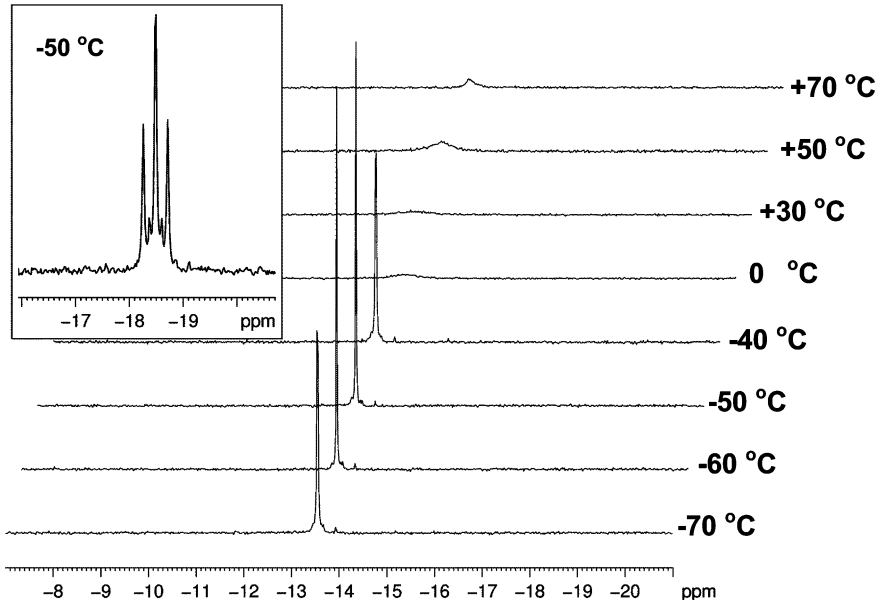

Figure 4. Variable-temperature ^{31}P NMR spectra of complex **1** in toluene-d_8. The inset shows the ^{31}P NMR spectrum at −50 °C after exchange with ^{13}CO.

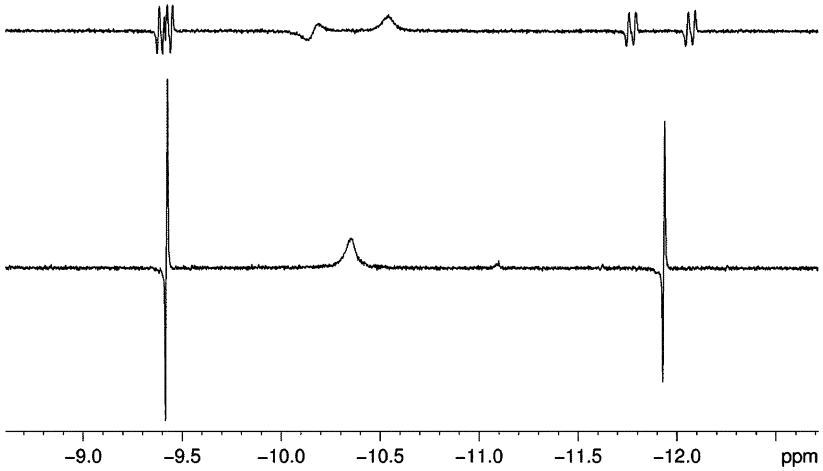

Figure 5. Hydride region of the ^1H (top) and $^1H\{^{31}P\}$ NMR spectra upon addition of *p*-H_2 to **1** at 50 °C in C_6D_6.

invoked to explain the dynamic behavior of **1-I** and the exchange of ^{13}CO for ^{12}CO. The dynamic behavior can be explained by reversible dissociation of one arm of the xantphos ligand, while CO exchange occurs by phosphine dissociation followed by ^{13}CO coordination, loss of ^{12}CO, and rechelation of the xantphos ligand. However, on the basis of the similarity of the dynamic behavior of **1-I** with that of $Ir(CO)(\eta^2\text{-}C_2H_4)_2(dppe)^{+}$[41] and the fact that dppe shows a greatly reduced tendency to dissociate, we favor the pseudorotation mechanism at low temperature.

Reaction of 1-X with Hydrogen. In benzene-d_6 at 50 °C, the reaction of **1-I** with para-enriched hydrogen results in the detection of *two* oxidative addition products showing PHIP effects (Figure 5). One product (**3-I**) exhibits a hydride signal at δ −11.91 that shows a coupling indicative of a hydride ligand trans to a phosphine donor, while the other hydride ligand is trans to carbonyl and provides a signal at δ −9.39. These observations are in agreement with previously reported observations for the kinetic dihydride product formed using IrI(CO)(dppe) and related systems.[30,31,34,42,43] The second dihydride product (**4-I**) exhibits a broad doublet at δ −10.35 in the ^1H NMR spectrum, with a separation of 161 Hz between the peak centers, although only the downfield component possesses clearly discernible emission/absorption (E/A) polarization. The acquisition of a $^1H\{^{31}P\}$ NMR spectrum of the reaction solution reveals that the major doublet splitting in **4-I** results from coupling to the ^{31}P nuclei (Figure 3, bottom) and quenches the antiphase character. We therefore conclude that **4-I**, which forms to an appreciable extent in solution, corresponds to an isomer of $IrH_2I(CO)$-(xantphos) in which both hydride ligands are trans to the two xantphos phosphorus donors (Scheme 2). On the basis of the concerted nature of the H_2 oxidative addition to d^8 square planar complexes, the observation of both **3-I** and **4-I** means that on CO elimination from **1-I**, two isomers of

(41) Albietz, P. J.; Cleary, B. P.; Paw, W.; Eisenberg, R. *Inorg. Chem.* **2002**, *41*, 2095−2108.

(42) Duckett, S. B.; Field, L. D.; Messerle, B. A.; Shaw, W. J.; Soler, L. P. *J. Chem. Soc., Dalton Trans.* **2000**, 2251−2253.

(43) Eisenschmid, T. C.; McDonald, J.; Eisenberg, R.; Lawler, R. G. *J. Am. Chem. Soc.* **1989**, *111*, 7267−7269.

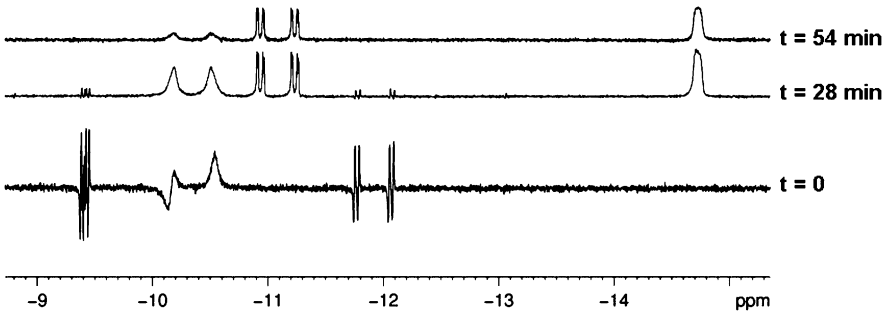

Figure 6. Hydride region of ^{1}H NMR spectra showing loss of polarization in the initially formed products and formation of the thermodynamically favored product over time upon addition of *p*-H_2 to **1** at 50 °C in C_6D_6.

Scheme 2

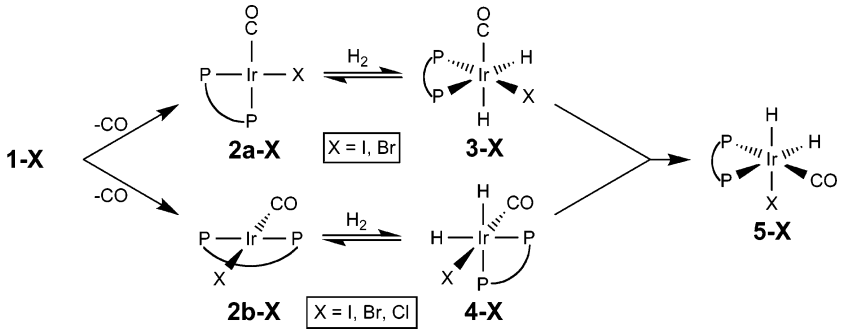

2-I form, one with the chelating phosphine donors cis to each other and the other with the xantphos phosphines mutually trans (**2b-I**). Oxidative addition to the latter isomer with the H_2 molecular axis parallel to the P−Ir−P axis thus yields **4-I**. In contrast, the addition of H_2 to **2b-I** with H_2 parallel to I−Ir−CO is precluded by unfavorable steric interactions between iodide, CO, and xantphos that would develop as iodide and CO attempt to move into mutually cis coordination positions during the concerted oxidative addition reaction. While the trans-spanning mode of the xantphos ligand, as written, suggests requisite coordination of the xanthene oxygen,[44−46] which in the present case would lead to a coordinatively saturated system, the structural results for **1-I**, **1-Br**, and **1-Cl** show that the Ir xantphos chelate ring is distinctly nonplanar, having an envelope conformation, and that the xanthene O atom is not required to bind to the Ir(I) center.

With regard to the polarized resonances of **4-I**, the separation between the two components in the polarized doublet at δ −10.35 is not simply due to a J_{PH} coupling because the absorption maxima of the resonances when polarized are separated by 176 Hz (Figure 6, bottom), whereas when the system is fully relaxed (Figure 6, middle), the splitting is 161 Hz. The results suggest that the PHIP intensities come from a second-order effect caused by the creation of an [AA′XX′] spin system[47] for the pair of chemically equivalent protons. While the configuration seen in **4-I** has not been observed previously in H_2 oxidative addition to $IrX(CO)L_2$ complexes where L_2 is a bidentate ligand, it has been seen before in a minor product through *p*-H_2 addition to *trans*-$IrCl(CO)(PPh_3)_2$.[48,49]

The reaction of **1-Br** with hydrogen is similar to that of **1-I** and requires modest heating for the dissociation of CO to generate the coordinatively unsaturated species IrBr(CO)(xantphos) (**2-Br**). On the other hand, the reaction of **1-Cl** with para hydrogen yields initially only the product in which both hydride ligands are trans to phosphorus (**4-Cl**), while **3-Cl** is never observed. Complex **4-Cl** is quite stable, and a preparative-scale synthesis was carried out, allowing for the isolation of crystals for an X-ray diffraction study. The X-ray diffraction study confirms the geometry of **4-Cl** (see Figure 7) and shows disorder (72:28) between the mutually trans chloride and carbonyl ligands. (Since the xantphos ligand dominates the packing in the solid state, the Ir position exhibits a concomitant disorder as well.) Tables 1 and 5 show the crystallographic details. The dominant packing form has the chloride ligand on the *same* side of the molecule as the xantphos backbone, in contrast with the structure of **1-Cl** where the chloride is on the opposite side. Consistent with the two packing forms in the X-ray structure, low-temperature ^{1}H and ^{31}P{^{1}H} NMR spectroscopy of the isolated chloro dihydride complex **4-Cl** show the presence of two isomeric dihydrides in a 5.6:1 ratio at −40 °C, both of which

(44) Sandee, A. J.; van der Veen, L. A.; Reek, J. N. H.; Kamer, P. C. J.; Lutz, M.; Spek, A. L.; van Leeuwen, P. W. N. M. *Angew. Chem., Int. Ed.* **1999**, *38*, 3231−3235.
(45) Zuideveld, M. A.; Swennenhuis, B. H. G.; Boele, M. D. K.; Guari, Y.; van Strijdonek, G. P. F.; Reek, J. N. H.; Kamer, P. C. J.; Goubitz, K.; Fraanje, J.; Lutz, M.; Spek, A. L.; van Leeuwen, P. W. N. M. *J. Chem. Soc., Dalton Trans.* **2002**, 2308−2317.
(46) Nieczypor, P.; van Leeuwen, P. W. N. M.; Mol, J. C.; Lutz, M.; Spek, A. L. *J. Organomet. Chem.* **2001**, *625*, 58−66.
(47) Emsley, J. W.; Feeney, J.; Sutcliffe, L. H. *High-Resolution Nuclear Magnetic Resonance Spectroscopy*; Pergamon Press: London, 1965.
(48) Hasnip, S. K.; Colebrooke, S. A.; Sleigh, C. J.; Duckett, S. B.; Taylor, D. R.; Barlow, G. K.; Taylor, M. J. *J. Chem. Soc., Dalton Trans.* **2002**, 743−751.
(49) Hasnip, S. K.; Duckett, S. B.; Sleigh, C. J.; Taylor, D. R.; Barlow, G. K.; Tayor, M. J. *Chem. Commun.* **1999**, 1717−1718.

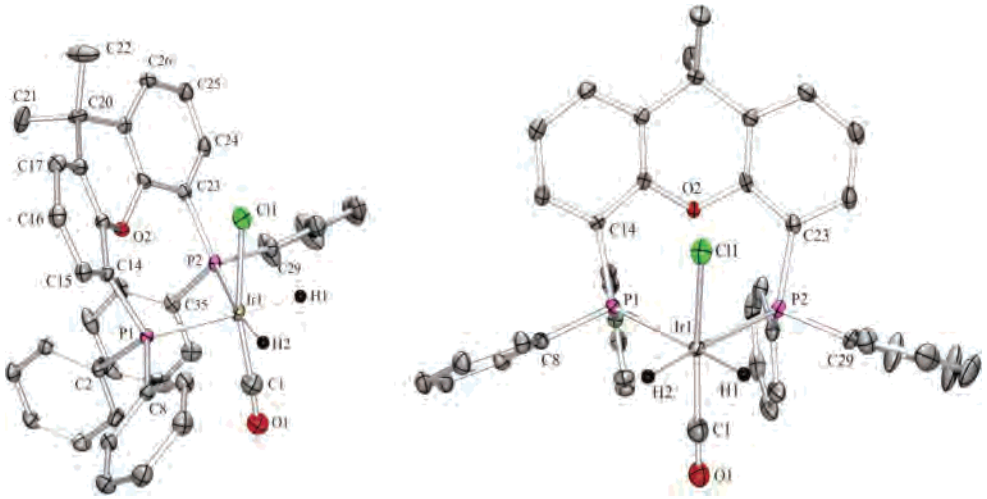

Figure 7. Two ORTEP views of **4-Cl** showing a partial labeling scheme; ellipsoids are at the 50% probability level. Hydrogen atoms other than the hydride ligands have been removed for clarity.

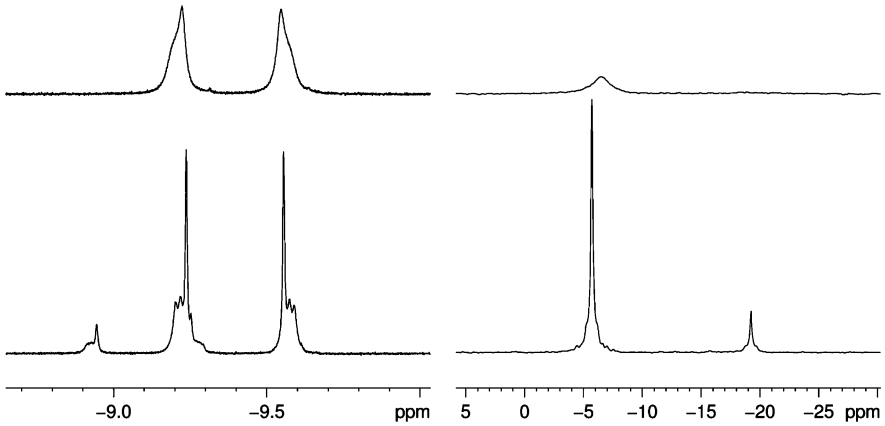

Figure 8. ^{1}H NMR spectra (left) and ^{31}P NMR spectra (right) of **4-Cl** at 25 °C (top) and −40 °C (bottom) in CD_2Cl_2.

Table 5. Selected Bond Lengths (Å) and Angles (deg) for the Major Form of **4-Cl**

Ir(1)−C(1)	1.877(8)	Ir(1)−H(1)	1.56
Ir(1)−Cl(1)	2.3980(16)	Ir(1)−H(2)	1.56
Ir(1)−P(1)	2.4231(7)	C(1)−O(1)	1.078(8)
Ir(1)−P(2)	2.4250(7)		
C(1)−Ir(1)−Cl(1)	167.8(4)	P(1)−Ir(1)−H(1)	166.5
C(1)−Ir(1)−P(1)	98.0(4)	P(2)−Ir(1)−H(1)	89.0
Cl(1)−Ir(1)−P(1)	91.59(6)	C(1)−Ir(1)−H(2)	86.5
C(1)−Ir(1)−P(2)	94.9(4)	Cl(1)−Ir(1)−H(2)	86.8
Cl(1)−Ir(1)−P(2)	90.34(6)	P(1)−Ir(1)−H(2)	85.2
P(1)−Ir(1)−P(2)	102.27(2)	P(2)−Ir(1)−H(2)	172.1
C(1)−Ir(1)−H(1)	88.2	H(1)−Ir(1)−H(2)	83.3
Cl(1)−Ir(1)−H(1)	80.9		

possess two hydrides that are trans to phosphorus (Figure 8). As with complex **1-Cl**, there is an apparent π-stacking interaction between two phenyl groups of the xantphos ligand, with a separation of 3.6 Å.

An alternative mechanism to rationalize the formation of **4-X** is illustrated in Scheme 3 and involves dechelation of the xantphos ligand in **1-X** to give a four-coordinate 16-electron species with a monodentate xantphos ligand, which then adds hydrogen, followed by rechelation of the xantphos ligand with loss of CO to generate **4-X** (as well as **3-X**). This mechanism cannot be ruled out without additional experiments including determination of the rate law for the reaction and its dependence on H_2 pressure. It is noteworthy that if this mechanism were operative, it would rule against dechelation of xantphos as the mechanism to explain the fluxional behavior of **1-X** since this would mean that the H_2 addition reaction should occur readily at ambient temperature, which it does not.

HMQC experiments confirm the $^{1}H-^{31}P$ and $^{31}P-^{31}P$ couplings of **3-X** and **4-X** (X = I, Br) in this reaction system. It is notable that over longer time periods at 50 °C, both dihydride isomers, **3-X** and **4-X** (X = I, Br), convert cleanly to a more stable isomer (**5-X**), in which the hydride ligands are trans to phosphorus and iodide, in approximately 2 h (Scheme 2, Figure 6). Analogous thermodynamic product isomers in H_2 oxidative addition have been described previously for reactions involving IrX(CO)(dppe) and related systems.[50,51] The chloride complex **4-Cl** behaves somewhat differently, with conversion from **4-Cl** to **5-Cl** requiring heating at 90 °C for 1 day.

Synthesis and Characterization of Trihydride and Acyl Complexes. The reaction of complex **1-I** with $NaBH_4$[39] at ambient temperature yields a mixture of $IrH(CO)_2$(xantphos) (**6**) and IrH_3(CO)(xantphos) (**7**) in a 1.4:1 ratio, and pho-

(50) Johnson, C. E.; Fisher, B. J.; Eisenberg, R. *J. Am. Chem. Soc.* **1983**, *105*, 7772−7774.
(51) Johnson, C. E.; Eisenberg, R. *J. Am. Chem. Soc.* **1985**, *107*, 3148−3160.

Scheme 3

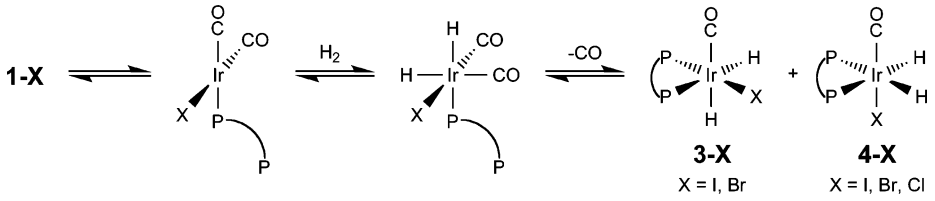

Scheme 4

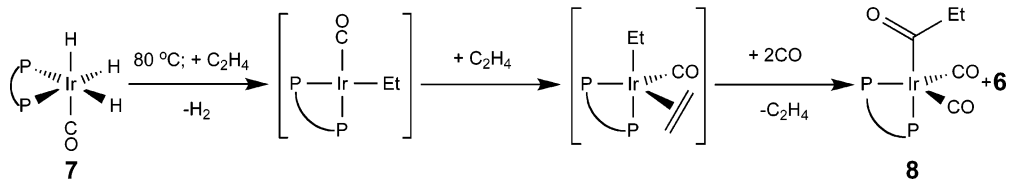

tolysis of the product mixture under 2 atm of H_2 gives trihydride **7** cleanly (eq 2). The resonance in the ^{1}H NMR spectrum corresponding to the hydride ligands trans to the two phosphorus donors of the xantphos ligand consists of a second-order pattern similar to that of the dppe analogue (Figure 9, top).[39] When the reaction of a sample of **7** with

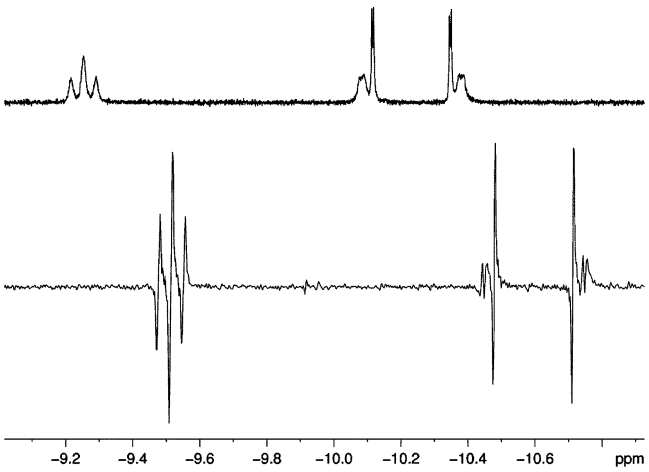

Figure 9. (top) Hydride region of the ^{1}H NMR spectrum of **7** at room temperature in C_6D_6. (bottom) Hydride region of the ^{1}H NMR spectrum of **7** upon addition of *p*-H_2 at 80 °C in C_6D_6.

p-H_2 is monitored by ^{1}H NMR spectroscopy at 80 °C, the hydride signals show polarization (Figure 9, bottom), indicating exchange with free *p*-H_2: no polarization is seen at temperatures lower than 70 °C, consistent with the view that a thermally driven reductive elimination of H_2 is necessary for exchange between the trihydride and free dihydrogen.

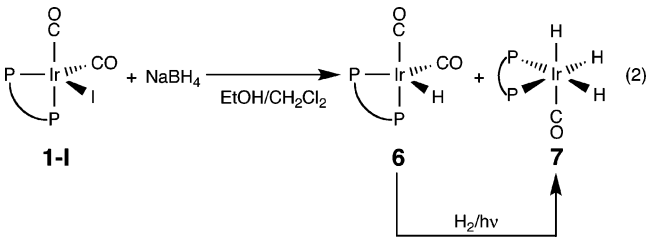

The acyl complex Ir(COEt)$(CO)_2$(xantphos) (**8**) is synthesized from trihydride **7** via the sequence shown in Scheme 4 that, based on previous work with the dppe analogue of **7**,

Table 6. Selected Bond Lengths and Angles for **8**

Ir(1)−C(1)	1.864(4)	Ir(1)−P(2)	2.4191(12)
Ir(1)−C(2)	1.945(4)	C(1)−O(1)	1.189(5)
Ir(1)−C(3)	2.104(4)	C(2)−O(2)	1.131(5)
Ir(1)−P(1)	2.4172(12)	C(3)−O(3)	1.227(6)
C(1)−Ir(1)−C(2)	132.37(17)	P(1)−Ir(1)−P(2)	101.05(4)
C(1)−Ir(1)−C(3)	87.81(19)	C(36)−P(1)−Ir(1)	115.46(11)
C(2)−Ir(1)−C(3)	87.03(17)	C(12)−P(1)−Ir(1)	118.79(12)
C(1)−Ir(1)−P(1)	87.01(14)	C(6)−P(1)−Ir(1)	113.08(12)
C(2)−Ir(1)−P(1)	89.98(12)	C(24)−P(2)−Ir(1)	112.96(12)
C(3)−Ir(1)−P(1)	169.80(12)	C(18)−P(2)−Ir(1)	116.60(12)
C(1)−Ir(1)−P(2)	118.42(13)	C(30)−P(2)−Ir(1)	119.63(11)
C(2)−Ir(1)−P(2)	108.81(12)	O(1)−C(1)−Ir(1)	174.4(4)
C(3)−Ir(1)−P(2)	89.14(13)	O(2)−C(2)−Ir(1)	171.3(4)

involves an ethyl ethylene complex.[16] Crystals of **8** suitable for X-ray diffraction were grown by vapor diffusion of pentane into a toluene solution at −35 °C. The geometry of **8**, which is shown in Figure 10, is a distorted trigonal bipyramid, as expected based on the related dppe complex,[16] with one phosphorus donor in an equatorial position, the other phosphorus donor axial, and the propionyl group in the other axial position. Tables 1 and 6 list the crystallographic details. The most striking difference between the structure of **8** and that of Ir(COEt)$(CO)_2$(dppe) is the P−Ir−P bond angle, which is 101.06° in **8** and 83.71° in the dppe complex.[16] In other respects, the structures are very similar. However, while the Ir−C(O) bond lengths are virtually identical in the dppe complex (1.869 and 1.870 Å), they are significantly different in **8** (1.864 and 1.944 Å). While the structures of **1-I** and **8** are both trigonal bipyramidal with one phosphine ligand equatorial and the other axial, the major difference between them is the fact that in **1-I** the iodide ligand occupies an equatorial position, while in **8** the anionic propionyl ligand is axial. The P−Ir−P angles are similar in the two structures (100.29° for **1-I** and 101.06° for **8**), and the sum of the three equatorial bond angles in each is within one degree of 360°, demonstrating the coplanarity of the equatorial ligands.

The NMR spectra of **8** indicate fluxional behavior in solution: the propionyl ethyl resonances in the ^{1}H NMR spectrum are broad, and only one broad resonance is seen in the ^{31}P{^{1}H} spectrum. A variable-temperature NMR study shows that **8** undergoes fluxional behavior similar to that of iodide complex **1-I** (vide supra). When the temperature is

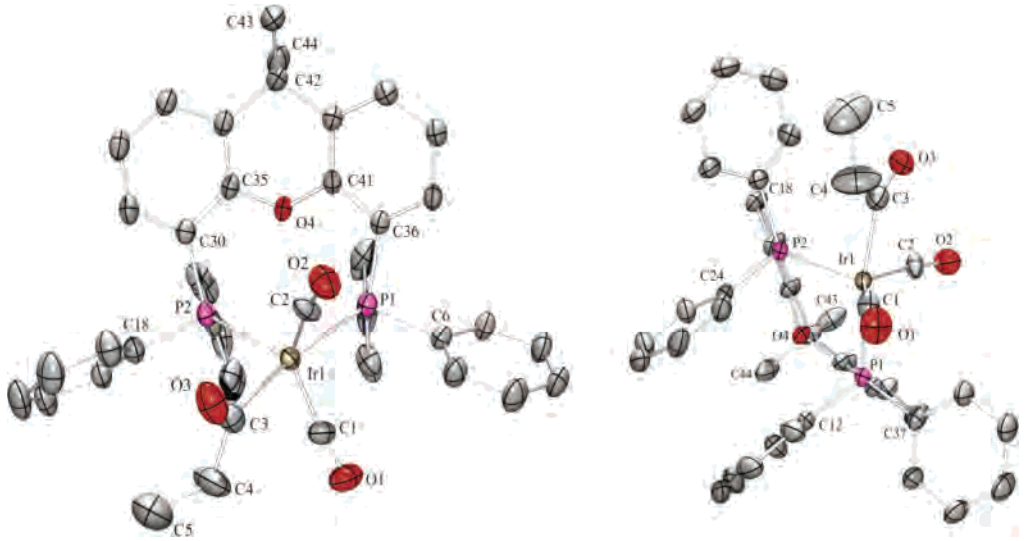

Figure 10. Two ORTEP views of **8** showing a partial labeling scheme; ellipsoids are at the 50% probability level. Hydrogen atoms have been removed for clarity.

lowered from 25 to 0 °C, the single phosphorus resonance of **8** sharpens, and coupling in the broadened propionyl ethyl resonances (J_{HH} = 7.1 Hz) becomes observable in the ^{1}H NMR spectrum. At −30 °C, the ^{31}P{^{1}H} spectrum once again displays only a broad signal, and no clear resonances are seen until −70 °C when two broad resonances appear. Further cooling to −80 °C gives better-resolved peaks at −15 and −24 ppm, consistent with the trigonal bipyramidal structure determined crystallographically (see Supporting Information). Additionally, the resonance corresponding to the two methyl groups on the xantphos backbone broadens as the temperature is lowered and then splits into two separate resonances at −50 °C. When the sample is cooled below −30 °C, the propionyl ethyl resonances rebroaden, although that of the CH_2 group becomes broad at higher temperature than does that of the CH_3 group. As with complex **1-I**, the fluxional behavior of **8** can be explained in terms of two processes: first, Berry pseudorotations with a lower-energy barrier and coalescence at −40 °C, and second, intermolecular CO ligand exchange with a higher-energy barrier seen by the broadening of resonances at 25 °C (vide supra).

Use of Ir(xantphos) Complexes as Hydroformylation Catalysts and Hydroformylation Model Systems. Complexes **6**, **7**, and **8** are catalysts for the hydroformylation of 1-hexene under 3 atm of a 2:1 mixture of H_2 and CO at 75 °C. The aldehyde is produced in about a 10% NMR yield after 24 h with a modest linear-to-branched ratio of 4 to 1. Over the same time period, alkene isomerization is competitive with hydroformylation such that >50% of the 1-hexene substrate is converted to internal isomers. The Ir(COEt)$(CO)_2$(dppe) complex also catalyzes 1-hexene hydroformylation with similar activity and linear-to-branched selectivity. Complete catalyst inhibition occurs in the presence of added xantphos (2-fold excess relative to iridium), such that no hydroformylation or alkene isomerization is observed. The catalyst inhibition suggests the possibility that xantphos dissociation may be necessary for catalysis to occur. A previous study of 1-hexene hydroformylation using $Ir_4(CO)_{12}$ as catalyst, albeit at higher temperature and pressure, showed higher yields of aldehyde (in part because of the harsher conditions) but with lower linear-to-branched selectivity.[14]

The Ir(xantphos) complexes are also catalysts for styrene hydroformylation, although the activity of these complexes is far lower than that of $RhH(CO)_2$(xantphos) generated in situ from $Rh(CO)_2$(acac) (1.4 vs 77% conversion after 20 h at 80 °C).[52] However, the linear-to-branched selectivity is higher using the iridium systems than rhodium (3.3:1 vs 1:1.6 after 20 h at 80 °C). The linear-to-branched selectivity observed with the iridium complexes is unusual because most hydroformylation catalysts yield more branched than linear products in the hydroformylation of styrene.[19−21,23] As with 1-hexene, hydroformylation catalysis by the iridium complexes is inhibited in the presence of the free xantphos ligand. The much lower rate of reaction when using an Ir(xantphos) catalyst rather than a rhodium analogue is consistent with the ability to observe acyl complexes **8** and IrH_2(COEt)(CO)(xantphos) (**9**) under noncatalytic conditions (vide infra). Under catalytic conditions, only monohydride **6** (or its dppe analog) is observed by NMR spectroscopy.

The addition of *p*-H_2 to acyl complex **8** at room temperature leads to polarized hydride resonances in the ^{1}H NMR spectrum corresponding to propionyl dihydride complex **9** (Figure 11a). Acyl dihydride species are intermediates in hydroformylation catalysis, and although these species have not been observed directly in catalytically active systems, they have been seen in model systems.[35,36] Over the course of 5 min, the polarization in the hydride resonances of **9** diminishes until the hydride signals are only just visible. Shaking of the NMR tube to dissolve more unreacted *p*-H_2 does not cause the polarized signals to return (Figure 11b), which is not unexpected because of the coordinative saturation of complex **8** which remains largely unreacted. However, upon heating of the sample to 70 °C, a return of polarization in the hydride resonances of **9** occurs along with conversion

(52) Note that there is 5% catalyst loading in the system, and therefore, 1.4% conversion is not strictly catalytic. Even if only small quantities of active catalyst are present, a very low number of turnovers is observed.

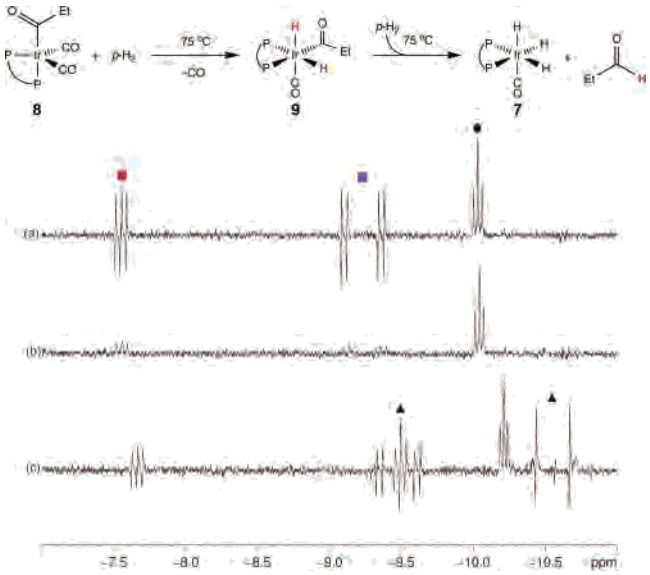

Figure 11. Hydride region of ^{1}H NMR spectra upon addition of p-H_2 to complex **8** in C_6D_6: (a) initial spectrum at 25 °C, (b) spectrum after shaking to redissolve p-H_2 once polarization had disappeared, and (c) spectrum after heating to 70 °C (■ = **9**, ▲ = **7**, and ● = **6**).

of **9** to form trihydride **7** and propanal (Figure 11c). The fact that polarization does not return *at room temperature* upon introduction of more p-H_2 into solution shows that the addition of p-H_2 to form dihydride **9** is not reversible at that temperature, indicating the likelihood that a small quantity of the four-coordinate Ir(COEt)(CO)(xantphos) is present initially to react with p-H_2 and form the dihydride species. As with complexes **1-X**, it is possible that a mechanism involving dechelation of xantphos prior to oxidative addition of dihydrogen is active in this system, but there is no direct evidence for it.

It is worth noting that, as **8** is consumed, the concentration of free CO increases and will compete for any open coordination sites on the Ir center, thus slowing the reaction with dihydrogen. Consistent with this hypothesis, the addition of p-H_2 to **8** in the presence of 1 atm CO does not lead to the polarized resonances corresponding to **9** until the sample is heated to 50 °C, at which temperature CO loss presumably occurs. Additionally, the dissociation of one of the two carbonyl ligands is effected by photolysis of **8** for 10 s outside the NMR spectrometer at room temperature in the presence of p-H_2, supporting a mechanism involving initial dissociation of CO; strongly polarized signals corresponding to **9** are immediately apparent when the ^{1}H NMR spectrum is recorded at ambient temperature. Both **8** and **9** are consumed completely after photolysis for longer periods to give trihydride **7** and propanal cleanly.

Interestingly, the ^{1}H NMR spectrum recorded upon reaction of **8** with p-H_2 at 80 °C shows the aldehydic proton of the propanal product in weak net *emission* (Figure 12). This effect (called oneH−PHIP because only one proton in the product aldehyde originates from a p-H_2 molecule) was observed previously in an analogous reaction with Ir(COEt)-$(CO)_2$(dppe).[35] The current result demonstrates that the oneH−PHIP effect might be more common and not limited to the specific conditions of a second-order effect in the

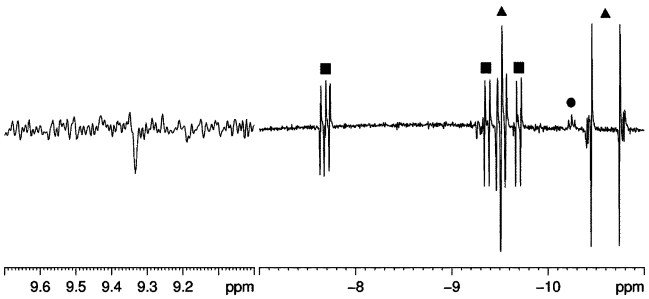

Figure 12. ^{1}H NMR spectrum showing polarization in the hydride resonances of acyl dihydride **9** and trihydride **7**, as well as the oneH−PHIP in the propanal product upon addition of p-H_2 to **8** at 75 °C in C_6D_6 (■ = **9**, ▲ = **7**, and ● = **6**).

overlapping hydride resonances of the intermediate acyl dihydride complex, which was proposed to be necessary in the earlier report.[35] The reaction of **8** with p-H_2 clearly shows that the hydride resonances of **9** are well separated such that there are no second-order effects (see Figures 11 and 12). The oneH−PHIP effect is observed in both benzene-d_6 and acetone-d_6 at temperatures ranging from 75 to 85 °C in the present system.

On the basis of these observations, the reaction of Ir(COEt)$(CO)_2$(dppe) with p-H_2 at 75 °C was re-examined on a 500 MHz NMR spectrometer to remove the second-order effects seen previously at 400 MHz, but oneH−PHIP was still seen to occur. The ^{1}H NMR spectrum clearly shows that the overlap observed in the hydride signals of IrH_2-(COEt)(CO)(dppe) at 400 MHz is nonexistent in the 500 MHz spectrum (see Supporting Information). Additionally, the experiment done under the same conditions, but with the acquisition of a ^{31}P-decoupled spectrum in which the two hydride resonances of IrH_2(COEt)(CO)(dppe) are well separated, also shows oneH−PHIP in the aldehyde product.

Conclusions

A new series of iridium complexes bearing the large natural bite angle xantphos ligand has been synthesized and studied, and five of the compounds have been characterized using X-ray diffraction. The trans-chelating ability of the xantphos ligand results in the formation of an unusual H_2 oxidative addition product upon addition of p-H_2 to **1-X** (X = I, Br, Cl). Variable-temperature NMR spectroscopy was used to examine the high- and low-temperature dynamic processes in complexes **1-I** and **8** that cause the interconversion of the two phosphine donors and the two methyl groups of the xantphos ligand. Parahydrogen-induced polarization was used to great effect to allow observation of propionyl dihydride complex **9**, and it also made the characterization of dihydrides **3-X**, **4-X**, and **5-X** by ^{1}H and ^{31}P NMR spectroscopy, including the use of two-dimensional techniques, possible. Additionally, polarization in the aldehyde product upon the reaction of para hydrogen with **8** and with Ir(COEt)$(CO)_2$(dppe) at different magnetic field strengths has shown that the unusual oneH−PHIP observation reported earlier is not limited to cases in which second-order effects exist in the hydride resonances of the model acyl dihydride intermediates. Finally, while complex **8** serves as a model

system for a key hydroformylation intermediate, **8**, **6**, and **7**, as well as Ir(COEt)$(CO)_2$(dppe), have been found to catalyze the hydroformylation of 1-hexene and styrene under mild conditions, but only modestly.

Experimental Section

General Considerations. Unless otherwise stated, all reactions and manipulations were performed in dry glassware under a nitrogen atmosphere using either standard Schlenk techniques or an inert-atmosphere glovebox. Styrene and 1-hexene were purchased from Aldrich and used without further purification. Benzene-d_6, acetone-d_6, dichloromethane-d_2, and toluene-d_8 were purchased from Cambridge Isotope Laboratories. THF, CH_2Cl_2, and toluene were purified as described by Grubbs.[53] All NMR spectra were recorded on either Bruker Avance 400 or 500 MHz spectrometers. ^{1}H NMR chemical shifts (in ppm) are relative to tetramethylsilane and referenced using chemical shifts of residual solvent resonances. ^{31}P NMR chemical shifts (in ppm) are relative to an external 85% solution of phosphoric acid in the appropriate solvent. The cis and trans designations in the assignments of phosphorus NMR signals are relative to the hydride ligands. $[Bu_4N][IrI_2(CO)_2]$,[38] [Ir(COD)Cl]$_2$,[40] Ir(COEt)$(CO)_2$(dppe),[16] Rh$(CO)_2$(acac),[54] and xantphos[23] were prepared as described previously. $[Bu_4N][IrBr_2(CO)_2]$ was prepared by heating to reflux a solution of K_3IrBr_6 in concentrated HBr and formic acid, followed by the addition of $[Bu_4N]$Br under inert atmosphere. Hydrogen enriched in the para spin state was prepared by the cooling of hydrogen over $FeCl_3$ adsorbed onto silica at 77 K.[55] Elemental analyses were performed by Desert Analytics, Inc.

Reactions with *p*-H_2. In a typical experiment, approximately 1−2 mg of sample was added to a J. Young NMR tube after which the desired solvent (∼0.6 mL) was added to the tube. The tube was degassed using three freeze−pump−thaw cycles and *p*-H_2 (ca. 3 atm at 298 K) was added to the tube while it was immersed in liquid N_2. The sample was thawed and shaken vigorously immediately before being inserted into the NMR probe heated to the desired temperature.

IrI$(CO)_2$(xantphos) (1-I). Complex **1-I** was synthesized using a procedure similar to that previously described for the synthesis of IrI(CO)(dppe).[38] Under an N_2 atmosphere, a solution of xantphos (777 mg, 1.34 mmol) in THF (25 mL) was added dropwise to a stirred solution of $[Bu_4N][IrI_2(CO)_2]$ (1.00 g, 1.34 mmol) in THF (50 mL), cooled to −78 °C. The yellow solution turned orange immediately upon the ligand addition. The mixture was stirred at −78 °C for 1 h, then allowed to warm to ambient temperature, and stirred an additional 2 h. The volume of the solution was reduced to 20 mL under vacuum, and 20 mL of degassed ethanol was added. The volume of the solution was reduced to 10 mL, resulting in the precipitation of an orange solid. The mixture was cooled to −35 °C in a freezer for several hours. The orange product was collected on a frit in air, washed with cold ethanol, hexanes, and diethyl ether (15 mL each), and dried in vacuo. Yield: 1.1 g (84%). Crystallization of **1-I** from dichloromethane layered with diethyl ether at −35 °C yielded orange blocks suitable for an X-ray diffraction study. ^{1}H NMR (C_6D_6, 400 MHz): δ 7.67 (br, phenyl, 8H), 7.09 (d, J_{HH} = 7.6 Hz, aryl, 2H), 6.92 (br, phenyl, 12H), 6.77 (t, J_{HH} = 7.6 Hz, aryl, 2H), 6.62 (br m, aryl, 2H), 1.37 (br, CH_3, 6H). ^{31}P{^{1}H} NMR (C_6D_6, 162 MHz): δ −13.5 (br). IR (KBr): 2029, 1948 cm^{-1}. Anal. Calcd for $C_{41}H_{32}IIrO_3P_2$: C, 51.64; H, 3.38. Found: C, 51.28; H, 3.52.

IrBr$(CO)_2$(xantphos) (1-Br). Complex **1-Br** was synthesized as described above for compex **1-I** using $[Bu_4N][IrBr_2(CO)_2]$ (500 mg, 0.77 mmol) as the starting material. Yield: 650 mg (93%). Crystals suitable for X-ray diffraction were obtained from a concentrated CH_2Cl_2 solution layered with pentane at −35 °C. The X-ray and NMR data were consistent with complex **1-Br** plus 0.5 equiv of dichloromethane, as was the elemental analysis. ^{1}H NMR ($CDCl_3$, 500 MHz, 25 °C): δ 7.60−7.00 (br m, 20H, phenyl), 7.50 (d, J_{HH} = 7.7 Hz, 2H, aryl), 7.11 (d, J_{HH} = 7.7 Hz, 2H, aryl), 6.38 (br, 2H, aryl), 1.58 (s, 6H, CH_3). ^{31}P{^{1}H} NMR (CD_2Cl_2, 203 MHz, 50 °C): δ −7.27 (s). IR (KBr): 2023, 1950 cm^{-1}. Anal. Calcd for $C_{41.5}H_{33}BrClIrO_3P_2$: C, 52.51; H, 3.50. Found: C, 52.48; H, 3.15.

IrCl$(CO)_2$(xantphos) (1-Cl). In a glovebox, a solution of xantphos (920 mg, 1.6 mmol) in CH_2Cl_2 (20 mL) was added to a stirred solution of $[Ir(COD)Cl]_2$ (540 mg, 0.80 mmol) also in CH_2Cl_2 (30 mL). CO was bubbled through the resulting yellow solution for 15 h. Volatile materials were then allowed to evaporate from the (now light orange) solution under an increased flow of CO. The resulting orange solid was crystallized from CH_2Cl_2 layered with pentane at −35 °C to give dark orange crystals, which were washed with pentane. The crystals were dried in vacuo to give **1-Cl** as an orange powder. Yield: 420 mg (30%). ^{1}H NMR (C_6D_6, 500 MHz, 25 °C): δ 8.01 (br m, 8H, phenyl), 7.22 (dd, J_{HH} = 7.7, 1.4 Hz, 2H, aryl), 7.04 (br m, 12H, phenyl), 6.91 (t, J_{HH} = 7.55 Hz, 2H, aryl), 6.78 (br, 2H, aryl), 1.51 (br s, 6H, CH_3). ^{31}P{^{1}H} NMR (C_6D_6, 203 MHz, 50 °C): δ 0.51 (s). IR (KBr): 2017, 1944 cm^{-1}. Anal. Calcd for $C_{41}H_{32}ClIrO_3P_2$: C, 57.11; H, 3.74. Found: C, 56.77; H, 3.49.

IrH_2Cl(CO)(xantphos) (4-Cl). IrCl$(CO)_2$(xantphos) (200 mg, 0.23 mmol) was dissolved in toluene (25 mL) and added to a glass vessel equipped with a Teflon stopcock and magnetic stir bar. The vessel was degassed and pressurized with 2 atm of H_2. The reaction mixture was heated at 70 °C for 1.5 h, resulting in a colorless solution and a yellow precipitate. The mixture was allowed to cool, and the supernatant was decanted from the yellow precipitate. The product was dissolved in CH_2Cl_2 and crystallized by layering the solution with diethyl ether at ambient temperature. The isolated golden crystals of **4-Cl** were washed with pentane and dried in vacuo. Yield: 120 mg (59%). ^{1}H NMR (CD_2Cl_2, 500 MHz, 25 °C): δ 7.7−7.5 (br, 4H, phenyl), 7.60 (br d, J_{HH} = 7.7 Hz, 2H, aryl), 7.5−7.2 (m, 14H, phenyl), 7.14 (td, J_{HH} = 7.7, 1.3 Hz, 2H, aryl), 6.34 (br, 2H, aryl), 1.88 (br s, 3H, CH_3), 1.60 (br s, 3H, CH_3), −9.39 (br d, 2H IrH_2). ^{31}P{^{1}H} NMR (CD_2Cl_2, 203 MHz, 50 °C): δ −6.49 (s). IR (KBr): 2123, 2083, 2017 cm^{-1}. Anal. Calcd for $C_{40}H_{34}ClIrO_2P_2$: C, 57.45; H, 4.10. Found: C, 58.07; H, 4.17.

IrH_2I(CO)(xantphos) (3-I). ^{1}H NMR (C_6D_6, 500 MHz, 50 °C): δ −9.39 (dd, J_{HP} = 13, 22 Hz, Ir*H*), −11.91 (dd, J_{HP} = 150, 18 Hz, Ir*H*). ^{31}P{^{1}H} NMR (C_6D_6, 203 MHz, 50 °C): δ −10.9 (br, Ir$P_{cis/cis}$), −26.1 (br, Ir$P_{trans/cis}$).

IrH_2I(CO)(xantphos) (4-I). ^{1}H NMR (C_6D_6, 500 MHz, 50 °C): δ −10.35 (br d, J_{HP} = 165 Hz). ^{31}P{^{1}H} NMR (C_6D_6, 203 MHz, 50 °C): δ −22.1 (s).

IrH_2I(CO)(xantphos) (5-I). ^{1}H NMR (C_6D_6, 500 MHz, 50 °C): δ −11.09 (dd, J_{HP} = 149, 25 Hz, Ir*H*), −14.73 (m, Ir*H*). ^{31}P{^{1}H} NMR (C_6D_6, 203 MHz, 50 °C): δ −15.4 (d, J_{PP} = 23 Hz, Ir$P_{cis/cis}$), −21.5 (d, J_{PP} = 23 Hz, Ir$P_{trans/cis}$).

(53) Pangborn, A. B.; Giardello, M. A.; Grubbs, R. H.; Rosen, R. K.; Timmers, F. J. *Organometallics* **1996**, *15*, 1518−1520.
(54) Hernandez-Gruel, M. A. F.; Perez-Torrente, J. J.; Ciriano, M. A.; Oro, L. A. *Inorg. Synth.* **2004**, *34*, 127−132.
(55) Millar, S. P.; Jang, M.; Lachicotte, R. J.; Eisenberg, R. *Inorg. Chim. Acta* **1998**, *270*, 363−375.

$IrH_2Br(CO)$(xantphos) (3-Br). ^1H NMR (C_6D_6, 500 MHz, 70 °C): δ −8.00 (dd, J_{HP} = 21, 14 Hz, Ir*H*), −10.91 (dd, J_{HP} = 159, 20 Hz, Ir*H*). $^{31}P\{^1H\}$ NMR (C_6D_6, 203 MHz, 80 °C): δ −19.6 (br, Ir$P_{trans/cis}$), −25.3 (br, Ir$P_{cis/cis}$).

$IrH_2Br(CO)$(xantphos) (4-Br). ^1H NMR (C_6D_6, 500 MHz, 70 °C): δ −9.22 (dd, J_{HP} = 188, 12 Hz, Ir*H*). $^{31}P\{^1H\}$ NMR (C_6D_6, 203 MHz, 70 °C): δ −15.8 (s).

$IrH_2Br(CO)$(xantphos) (5-Br). ^1H NMR (C_6D_6, 500 MHz, 80 °C): δ −10.71 (ddd, J_{HP} = 153, 26 Hz, J_{HH} = 5.4 Hz, Ir*H*), −16.61 (m, Ir*H*). $^{31}P\{^1H\}$ NMR (C_6D_6, 203 MHz, 80 °C): δ −9.57 (d, J_{PP} = 33 Hz, Ir$P_{cis/cis}$), −14.9 (d, J_{PP} = 31 Hz, Ir$P_{trans/cis}$).

$IrH_2Cl(CO)$(xantphos) (5-Cl). ^1H NMR (C_6D_6, 500 MHz, 80 °C): δ −10.13 (dd, J_{HP} = 157, 25 Hz, Ir*H*), −17.3 (m, Ir*H*). $^{31}P\{^1H\}$ NMR (C_6D_6, 203 MHz, 80 °C): δ −4.97 (br, Ir$P_{cis/cis}$), −9.92 (br, Ir$P_{trans/cis}$).

$IrH_3(CO)$(xantphos) (7). The preparation of **7** was carried out in a manner similar to the preparation of $IrH_3(CO)$(dppe) from IrI(CO)(dppe).[39] Under N_2 (nearly identical results were obtained under an H_2 atmosphere), a solution of $NaBH_4$ (280 mg, 7.3 mmol) in ethanol (50 mL) was added to a stirred solution of **1** (700 mg, 0.73 mmol) in dichloromethane (10 mL). The orange solution faded to colorless immediately upon addition of the $NaBH_4$ solution. The reaction mixture was stirred at ambient temperature for 1 h, after which 2 g of silica gel was added. The mixture was stirred until gas evolution ceased (~1 h). The silica gel was removed from the solution by filtration through a glass frit in air, and the product was washed through the frit with additional dichloromethane (10 mL). The solution was concentrated on a rotary evaporator to 10 mL, and the very pale yellow precipitate that formed was collected on a glass frit and washed with cold ethanol and diethyl ether (10 mL each). The crude product (a 1:0.7 mixture of **6** and **7**) was dissolved in 25 mL of toluene and added to a glass vessel with a Kontes stopcock and a magnetic stir bar. The vessel was degassed, and 2 atm of H_2 were added. The reaction mixture was photolyzed with an unfiltered 200 W mercury xenon lamp for 20 h to give clean **7**. Yield: 420 mg (71%). Crystallization from dichloromethane layered with diethyl ether at −35 °C yielded pure **7** as a light tan solid. ^1H NMR (C_6D_6, 500 MHz): δ 7.71 (br, phenyl, 4H), 7.60 (br, phenyl, 4H), 7.07 (d, J_{HH} = 7.95 Hz, aryl, 2H), 6.94 (br, phenyl, 6H), 6.9−6.7 (m, phenyl, 6H), 6.69 (td, J_{HH} = 7.74, 1.18 Hz, aryl, 2H), 6.49 (t, J_{HH} = 8.07 Hz, aryl, 2H), 1.43 (s, CH_3, 3H), 1.37 (s, CH_3, 3H), −9.37 (t, J_{HP} = 18.61 Hz, Ir*H*, 1H), −10.35 (ddd, J_{HP} = 129.62, 15.70 Hz, J_{HH} = 2.58 Hz, Ir*H*, 2H). $^{31}P\{^1H\}$ NMR (C_6D_6, 203 MHz): δ −8.62. IR (KBr): 2060 (ν_{IrH}), 2008 (ν_{IrH}), 1954 (ν_{CO}), 1917 (ν_{IrH}) cm^{-1}. Anal. Calcd for $C_{40}H_{35}IrO_2P_2$: C, 59.92; H, 4.40. Found: C, 59.63; H, 4.23.

Ir(COEt)$(CO)_2$(xantphos) (8). Complex **8** was synthesized using the method previously reported for the preparation of Ir(COEt)$(CO)_2$(dppe).[16] Trihydride **7** (600 mg, 0.75 mmol) was dissolved in toluene (30 mL) and heated at 80 °C with ethylene bubbling through the solution for 2 h. The golden solution was allowed to cool to room temperature and was stirred with CO bubbling through the solution for 20 h at ambient temperature. Ethanol (30 mL) was added to the golden solution, and the entire mixture was concentrated to ~5 mL by rotary evaporation. The tan powdery solid that precipitated from the solution was isolated from the supernatant solution and washed with cold ethanol (10 mL). NMR spectroscopy revealed the solid to be a mixture of the desired complex and **6** in a 1:1.5 ratio (525 mg). Crystals of sufficient quality for an X-ray diffraction study were obtained by vapor diffusion of pentane into a toluene solution of the product at −35 °C, but samples of sufficient purity for acceptable elemental analysis could not be obtained. ^1H NMR (C_6D_6, 500 MHz): δ 7.67 (br, phenyl, 8H), 7.00 (br, phenyl, 12H), 6.84 (m, aryl, 6H), 2.82 (br, C(O)CH_2CH$_3$, 2H), 1.46 (br, CH_3, 6H), 0.84 (br, C(O)CH$_2$CH_3, 3H). $^{31}P\{^1H\}$ NMR (C_6D_6, 203 MHz): δ −20.24 (s).

IrH_2(COEt)(CO)(xantphos) (9). ^1H NMR (C_6D_6, 500 MHz): δ −7.44 (t, J_{HP} = 18.80 Hz, Ir*H*, 1H), −9.12 (dd, J_{HP} = 128.79, 19.87 Hz, Ir*H*, 2H). $^{31}P\{^1H\}$ NMR (C_6D_6, 203 MHz): δ −11.8 (d, J_{PP} = 20.1 Hz, Ir$P_{trans/cis}$), −21.9 (d, J_{PP} = 22.6 Hz, Ir$P_{cis/cis}$).

Hydroformylation Reactions. In a typical experiment, a J. Young NMR tube was charged with $IrH_3(CO)$(xantphos) (3.1 mg, 0.0039 mmol), styrene (8.9 μL, 0.078 mmol) or 1-hexene (9.7 μL, 0.078 mmol), ferrocene as internal standard (1.0 mg, 0.0054 mmol), and benzene-d_6 (0.6 mL). The tube was degassed using three freeze−pump−thaw cycles, and CO (1 atm) was added. The tube was frozen in liquid N_2, and H_2 (~2 atm) was added. The reaction was heated in an oil bath at the desired temperature and monitored regularly by NMR spectroscopy.

Crystal Structure Determinations. For each structure determination, a crystal was placed onto the tip of a 0.1 mm diameter glass fiber and mounted on a Bruker SMART APEX II Platform CCD diffractometer for a data collection at 100.0(1) K, except for **8** (100(2) K). A preliminary set of cell constants was calculated from the reflections harvested from three sets of 12 (**1-I**, **1-Cl**) or 20 (**1-Br**, **4-Cl**, **8**) frames. These initial sets of frames were oriented such that orthogonal wedges of reciprocal space were surveyed. This produced initial orientation matrixes determined from 165 reflections. The data collection for each determination was carried out using Mo Kα radiation (graphite monochromator). A randomly oriented region of reciprocal space was surveyed to the extent of one sphere and to a resolution of 0.70−0.72 Å. Four major sections of frames were collected with 0.30° (**1-I**, **8**) or 0.50° (**1-Br**, **1-Cl**, **4-Cl**) steps in ω at four different ϕ settings and a detector position of −28° (**1-I**, **1-Cl**, **8**) or −33° (**1-Br**, **4-Cl**) in 2θ. The intensity data were corrected for absorption (SADABS).[56] Final cell constants were calculated from the *xyz* centroids of the strong reflections from the actual data collection after integration (SAINT).

Each structure was solved using SHELXS-97[57] and refined using SHELXL-97.[57] The space groups $P2_1/c$ for **1-X** (X = I, Br, Cl) and $P\bar{1}$ for **4-Cl** and **8** were determined. For each determination, a direct-methods solution was calculated which provided most non-hydrogen atoms from the E-map. Full-matrix least squares/difference Fourier cycles were performed which located the remaining non-hydrogen atoms. All non-hydrogen atoms were refined with anisotropic displacement parameters. All hydrogen atoms were placed in ideal positions and refined as riding atoms with relative isotropic displacement parameters. Unit cell, space group, data collection, and refinement parameters for all structures are summarized in Table 1.

Details for the Structure of 1-Br. All atoms lie in general positions. The axial carbonyl and bromide ligands are modeled as disordered with each other (84:16). Thermal constraints were applied to the disorder model. Highly disordered solvent is present in channels parallel to the *a* axis and appears to be dichloromethane. The reflection contibutions from this solvent were removed using the program PLATON, function SQUEEZE.[58]

Details for the Structure of 1-Cl. The chloride ligand is modeled as disordered with the axial carbonyl ligand (85:15). π-Stacking

(56) The SADABS absorption correction program is based on the method of Blessing; Blessing, R. H. *Acta Crystallogr. A* **1995**, *51*, 33−38.
(57) *SHELXTL: Structure Analysis Program*, version 5.04; Siemens Industrial Automation Inc.: Madison, WI, 1995.
(58) Spek, A. L. *PLATON*, version 300106; Utrecht University: Utrecht, The Netherlands, 2006; Spek, A. L. *Acta Crystallogr. A* **1990**, *46*, C34.

(∼3.6 Å) is likely present between two of the phenyl rings; the angle between their planes is 2.46(7)°.

Details for the Structure of 4-Cl. The chloride and carbonyl ligands are disordered with each other, such that the iridium atom is also disordered over two positions (72:28). Thermal constraints and geometrical restraints were applied to the disorder model. π-Stacking may be present: two of the phenyl rings are eclipsed with a distance of approximately 3.6 Å and an angle of 6.35(16)°.

Details for the Structure of 8. The asymmetric unit consists of one iridium molecule and one and a half toluene molecules. Toluene molecule C45−C51 is modeled as disordered over two positions (60:40), and toluene molecule C52−C58 is modeled as disordered over a crystallographic inversion center (50:50). Fixed geometries were applied to the benzene portions of both toluene molecules (AFIX 66).

Acknowledgment. We gratefully acknowledge Mr. Abdurrahman C. Atesin for helpful discussions and for providing $[Ir(COD)Cl]_2$, Dr. Mesfin Janka for helpful discussions, and Professor George G. Stanley for insightful comments. We also thank the National Science Foundation (Grant CHE-0092446) and the donors of the Petroleum Research Fund for support of this work.

Supporting Information Available: Crystal data, atomic coordinates, bond distances, bond angles, and anisotropic displacement parameters for **1-X** (X = I, Br, Cl), **4-Cl**, and **8** (in CIF format), as well as some NMR spectra. This material is available free of charge via the Internet at http://pubs.acs.org.

IC060731L